# Green Chemistry

Accepted Manuscript






ROYAL SOCIETY OF CHEMISTRY

www.rsc.org/greenchem

Cite this: DOI: 10.1039/c0xx00000x

www.rsc.org/greenchem PAPER

# Synthesis of highly dispersed metal sulfide catalysts via low temperature sulfidation in a dielectric barrier discharge plasma†

**Lu Zhao,[a] Yao Wang,*[a] Zhili Sun,[a] Anjie Wang,[a] Xiang Li,[a] Chunshan Song[a,b] and Yongkang Hu[a]**

***Received (in XXX, XXX) Xth XXXXXXXXX 20XX, Accepted Xth XXXXXXXXX 20XX***
**DOI: 10.1039/b000000x**

A new strategy is reported for synthesizing supported metal sulfides with high dispersion by sulfidation in a dielectric barrier discharge (DBD) plasma under ambient conditions. According to the characterization by XRD, BET, UV-vis, TEM, XPS, ICP, and elemental analysis, the DBD plasma method not only reduces the preparation time but also achieves an increased dispersion, small particle size and uniform distribution compared to the traditional thermal method. These results prove that the plasma preparation method is a facile and flexible approach for the synthesis of metal sulfides. The plasma-prepared $CdS/Al_2O_3$ and $ZnS/Al_2O_3$ catalysts exhibited a high performance for hydrogen production from $H_2S$ at reduced energy cost. The enhancement might be attributable to a smaller particle size, higher surface area and dispersion, which enhances the semiconductor catalytic efficiency.

## 1 Introduction

Metal sulfides are important materials because of their extensive applications in electronics, catalysis, optoelectronics, and magnetic devices.[1] A variety of methods for synthesizing semiconductor metal sulfides have been developed, including direct elemental reaction at high temperature,[2] chemical deposition reaction,[3] hydrothermal reaction,[4] solvothermal reaction,[5] ball mill solid-state metathesis reaction,[6] sonochemical reaction,[7] electrochemical reaction,[8] and thermal decomposition.[9] However, some of these methods require high temperatures, leading to sintering of the synthesized particles, whereas the others use toxic organometallic precursors. Supported metal sulfides are normally prepared by sulfidation of metal oxides with sulfur-containing compounds (such as $H_2S$ and $CS_2$) at elevated temperatures.[10] The transformation of a metal oxide to the metal sulfide is generally thermodynamically favorable, and the barriers for sulfidation of metal oxides are usually low.[11,12] Nonetheless, sulfidation proceeds considerably slowly at low temperature, and high temperatures are frequently needed. However, the high temperature process is energy-intensive, and may lead to the sintering of the synthesized metal sulfide particles and thus a lower dispersion in the supported catalysts.

Recently, non-thermal plasma techniques have attracted growing attention in the field of supported catalysts preparation. Compared with thermal approaches, plasma techniques have the advantages of shorter preparation time and lower energy requirements, and the obtained supported catalysts have smaller particle size of the active phase with higher dispersion and higher catalytic activities. According to Zhu et al.[13], instead of conventional calcination and reduction, supported $H_2PtCl_6$ was treated by non-thermal plasma at room temperature, and the plasma-reduced $Pt/Al_2O_3$ catalyst exhibited smaller particle size and higher platinum dispersion than a conventionally prepared $Pt/Al_2O_3$ catalyst. He et al.[14] used a cold $H_2$ plasma to synthesize reduced noble metal nanoparticles supported on $TiO_2$-gel films and controlled the particle sizes between 2 and 10 nm. Chu et al.[15] and Hong et al.[16] have recently prepared alumina- and silica-supported Co catalysts using a glow discharge plasma. They reported increased Co dispersion when decomposition of cobalt nitrate was conducted using plasma instead of thermal calcination. Liu et al.[17] reported a $Ni/SiO_2$ catalyst prepared by non-thermal plasma, instead of by thermal reduction in hydrogen, for the methane reforming reaction. The methane conversion and $CO_2$ conversion could reach 93% and 76%, respectively, over the $Ni/SiO_2$ catalyst prepared by this method. Hua et al.[18] developed a method to prepare a Ni/MgO catalyst in one step through the plasma treatment of co-precipitated $NiCO_3$-$MgCO_3$. In this way, the MgO support and Ni active component were simultaneously prepared, and more than 20% higher conversions of methane and carbon dioxide were obtained than over the conventional Ni/MgO catalyst.

In this paper, supported metal sulfides were prepared from their precursors by sulfidation in a $H_2S$-containing plasma. The obtained metal sulfides were characterized by means of XRD,

[a] *Key Laboratory of Industrial Ecology and Environmental Engineering (MOE), PSU-DUT Joint Center for Energy Research, School of Chemical Engineering, Dalian University of Technology, Dalian 116024, P.R. China. E-mail: wangyao@dlut.edu.cn; Fax: (+86) 411 8498 6121; Tel: (+86) 411 8498 6121*
[b] *EMS Energy Institute, Department of Energy and Mineral Engineering, The Pennsylvania State University, C211 CUL, University Park, PA 16802-2323, USA.*
† Electronic supplementary information (ESI) available. See DOI: 10.1039/b000000x/

BET, UV-vis, TEM, XPS, ICP, and elemental analysis, and compared with the metal sulfides prepared by thermal sulfidation. The catalytic performances of $CdS/Al_2O_3$ and $ZnS/Al_2O_3$ prepared by two different methods were comparatively investigated in the plasma-induced $H_2S$ decomposition.

## 2 Experimental section

### 2.1 Synthesis of supported metal sulfides

$Al_2O_3$-supported metal sulfide precursors were prepared by impregnation from their salts and $Al_2O_3$. $\gamma$-$Al_2O_3$ extrudes (surface area: 270 $m^2/g$) were crushed and sieved to 40-60 mesh. A loading level of 10 wt% oxide precursor was chosen for each catalyst, unless otherwise specified. $Cd(NO_3)_2$ and $Zn(NO_3)_2$ were used in the preparation of CdS and ZnS. Metal salts were dissolved in 12 mL de-ionized water. The resulting solution was mixed with 12 g $\gamma$-$Al_2O_3$ particles, and kept at room temperature for 8 h. Then the mixture was dried in an oven at 120 °C for 12 h. The obtained sample was divided into four parts. The first part was calcined at 450 °C in air for 5 h and then sulfided in a 10% $H_2S$/Ar flow (80 mL/min) at 400 °C for 3 h (marked as CTS); the second part was directly thermally sulfided at 400 °C in 10% $H_2S$/Ar (80 mL/min) for 3 h (marked as TS); the third part was calcined at 450 °C for 5 h and then sulfided using the non-thermal plasma (marked as CPS); the fourth part was directly decomposed and sulfided using the non-thermal plasma (marked as PS). The setup applied for the DBD plasma has been described previously in detail.[19] The structure of the reactor mainly consisted of a quartz tube and two electrodes. The high-voltage electrode was a stainless-steel rod with a diameter of 2.5mm, which was installed along the axis of the quartz tube and connected to an alternating current supply. The grounding electrode was an aluminum foil, which was wrapped around the quartz tube and linked to ground by a wire. For each run, two grams of the precursor was placed into the gap between the quartz tube and the high-voltage electrode, and 10% $H_2S$/Ar was allowed to pass through the bed at 80 mL/min. The total input of the AC power was about 25 W in a steady state. The voltage of the high-voltage electrode was kept at around 10 kV and the discharge frequency at 10 kHz. The plasma sulfidation time was 10 min. To confirm the low temperature process, infrared (IR) imaging (Thermovision A40 M) was used to measure the temperature distribution of the cross section of the reactor under actual conditions in $H_2S$ plasma sulfidation. Fig. S1 (ESI†) shows that the bed temperature was around 150 °C during the plasma sulfidation. As a result, the thermal effect during the DBD plasma sulfication could be ignored.

To further prove the feasibility of the $H_2S$ plasma method in synthesizing metal sulfides, we applied this approach to synthesize other metal sulfides. The XRD patterns (Fig. S2, ESI†) show that supported CoS, $FeS_2$, $Ag_2S$, MnS, NiS, $MoS_2$, CuS and $WS_2$ were readily obtained from their salt precursors by this approach.

### 2.2 Characterization

The XRD patterns of the samples were measured on a Rigaku D/Max 2400 diffractometer using nickel-filtered Cu Kα radiation at 40 kV and 100 mA. The BET surface areas of the metal sulfide catalysts were measured by $N_2$ adsorption at liquid $N_2$ temperature using a Micromeritic TriStarII 3020 instrument. UV–visible spectroscopy measurement was carried out on a Jasco V-550 spectrophotometer, using $BaSO_4$ as the reference sample. Transmission electron microscope (TEM) images of the samples were acquired on a JEM-2100 microscope operating at 200 kV. X-ray photoelectron spectra (XPS) were acquired with a Multilab-2000 X-ray photoelectron spectrometer, using an Al Kα source. All binding energies were referenced to the C 1s peak at 284.6 eV. Chemical composition of the catalysts were analyzed by inductively coupled plasma-atomic emission spectroscopy (ICP-AES) using an Optima 2000 DV spectrometer. Elemental analysis was carried out using Vario EL III CHNOS elemental analyzer.

### 2.3 Catalystic performance

The process of $H_2S$ decomposition in a non-thermal plasma aided by semiconductor catalysts has been illustrated in detail in our previous study.[20,21] 15.0 mL of the supported catalyst was charged into the reactor. The reactor was immersed in an oil bath, which was kept at 120 °C. A flow of 20% $H_2S$ in Ar (30 mL/min) was passed through the catalyst bed while a head-to-head voltage (10 kHz) was applied to generate a non-thermal plasma by DBD. The effluent was passed through a saturated NaOH solution trap to remove unreacted $H_2S$, and the hydrogen content was analyzed by an on-line gas chromatograph equipped with a thermal conductivity detector. At 100% conversion, the effluent was re-checked with lead acetate test paper.

In $H_2S$ decomposition, only $H_2$ and S are produced, without any other byproduct. Therefore, $H_2S$ conversion ($x_{H2S}$) is equivalent to $H_2$ yield ($Y_{H2}$):

$$x_{H2S} = Y_{H2} = \frac{A_E}{A_0} \times 100\%$$

Where $A_E$ is the $H_2$ peak area in the chromatogram of the effluent, $A_0$ is the $H_2$ peak area at full $H_2S$ conversion.

The area of the Lissajous diagram measures the energy dissipated in the discharge during one period of the voltage. The charge was determined by measuring the voltage across the capacitor of 0.47 μF connected in series to the ground line of the plasma reactor.[22] The discharge power was calculated from the product of the area of charge–voltage parallelogram and the frequency of discharge (10 kHz). Specific input energy (SIE, J/L), which measures the energy input in the plasma process, was calculated by:

$$SIE = \frac{P}{V}$$

where P is the discharge power (W), and V is the gas flow rate (L/s).

The energy consumption for hydrogen production (E, eV) was calculated from SIE, $H_2$ yield, and initial $H_2S$ concentration (20%):

$$E = \frac{SIE}{Y_{H2} \cdot 20\%} \times \frac{22.4}{96}$$

## 3 Results and discussion

### 3.1 XRD analysis

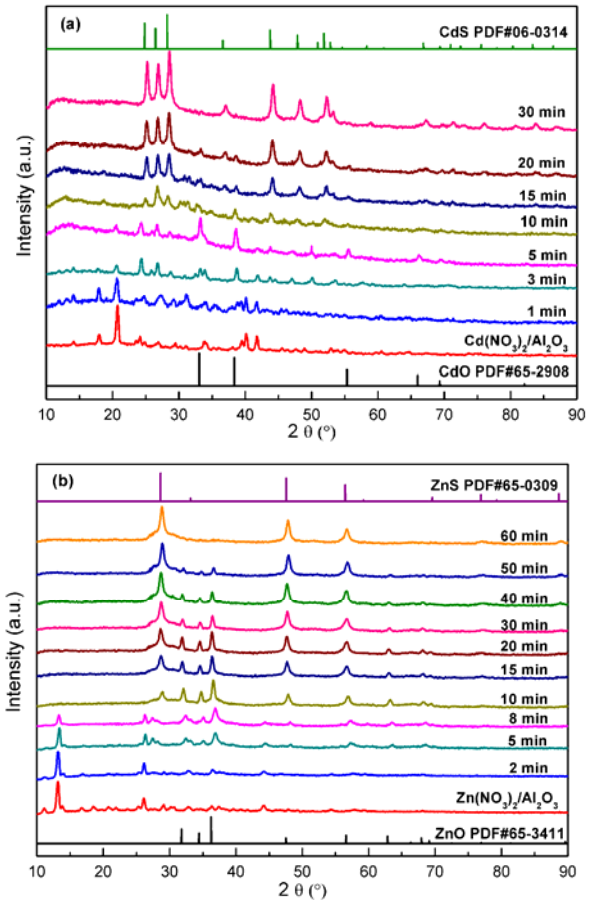


**Fig. 1** XRD patterns of $Cd(NO_3)_2/Al_2O_3$ (a) and $Zn(NO_3)_2/Al_2O_3$ (b) sulfided by the $H_2S$ plasma at various times. The loading level of the metal salts was 60 wt%. The total input of the AC power was 25 W.

In a non-thermal plasma, high-energy electrons collide inelastically with $H_2S$ molecules in the plasma and transfer their energy to the molecules, which leads to the production of excited $H_2S$ molecules, SH species and ions.[23] Liu et al.[24,25] reported that the bonds of the metal salt precursors or clusters are potentially distorted or elongated and are easily split if they collide with other energetic species in a plasma. Therefore, the metal salt precursors can be converted into metal sulfides in the $H_2S$ plasma under mild conditions.

Fig. 1 represents the XRD patterns of the metal salt precursors recorded at different times when $H_2S$ plasma sulfidation was performed. In order to observe the variations clearly, a loading level of 60 wt% salt precursor was chosen. Fig. 2 indicates that complete decomposition of the salt precursors into metal oxides could be achieved in a short period of time and then metal oxides are sulfided. As shown in Fig. 1(a), the peaks of $Cd(NO_3)_2$ almost disappeared in only 10 min, and completely vanished in 20 min. Meanwhile, the intensity of the diffraction peaks of the generated CdO phase decreased and a new phase of CdS appeared and increased with the discharge time. It indicates that metal oxides generated from decomposed salt precursors were sulfided in the $H_2S$ plasma. Moreover, the intensity of the main diffraction peaks of the metal sulfides increased with increasing discharge time, indicating that the degree of crystallinity of the sulfides became higher. In contrast, as shown in Fig 1(b), $Zn(NO_3)_2$ decomposed faster. The peaks of $Zn(NO_3)_2$ completely disappeared in 10 min. During discharge, the peak intensities of ZnO also decreased gradually, and the diffraction peaks completely vanished in 60 min. Simultaneously, the ZnS phase appeared and its peak intensities notably increased with increasing discharge time. In summary, the analysis of the XRD patterns confirmed the complete chemical conversion of the salt precursors into metal sulfides.

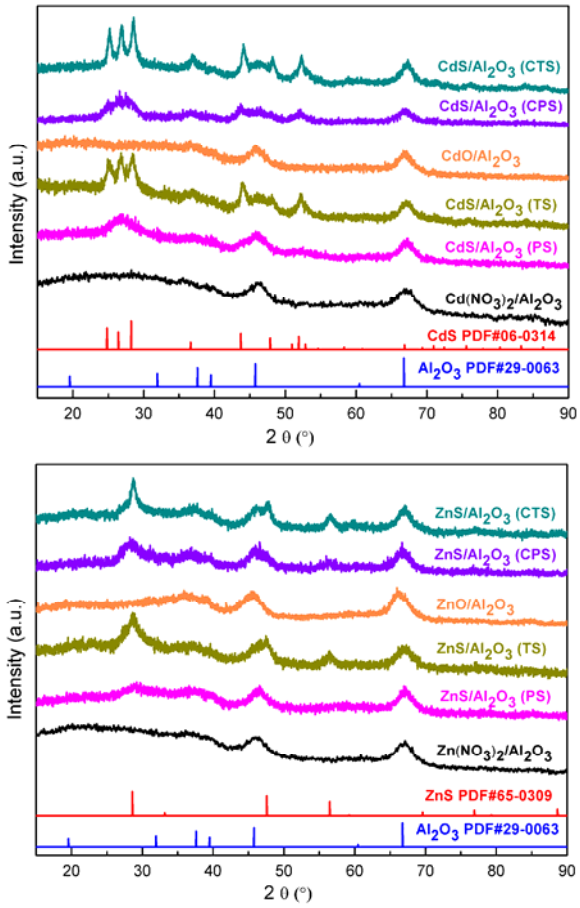


**Fig. 2** XRD patterns of $CdS/Al_2O_3$ and $ZnS/Al_2O_3$ synthesized with different methods.

Fig. 2 shows the XRD patterns of the supported nitrate precursors, oxide precursors and metal sulfides prepared via different methods for $CdS/Al_2O_3$ and $ZnS/Al_2O_3$. In the patterns of the supported metal nitrates or metal oxides, only the diffraction peaks of the alumina were detected, and no other diffraction peaks were detectable. The CdS characteristic peaks of $CdS/Al_2O_3$ (CPS) and $CdS/Al_2O_3$ (PS) were broader and weaker than those of $CdS/Al_2O_3$ (CTS) and $CdS/Al_2O_3$ (TS), which indicated that the particle size of CdS prepared by the plasma method was smaller. According to the Scherrer equation, as shown in Table 1, the particle sizes of $CdS/Al_2O_3$ (CTS) and $CdS/Al_2O_3$ (TS) catalyst were 10.7 and 10.5 nm, respectivelly, whereas that of the plasma-prepared samples (CPS) was 8.1 nm. The CdS particle size of $CdS/Al_2O_3$ (PS) was even smaller (6.7 nm). A similar trend was observed for the $ZnS/Al_2O_3$ samples.

The particle size of ZnS was 7.5 nm for ZnS /$Al_2O_3$ (CPS) and 6.2 nm for ZnS /$Al_2O_3$ (PS). This also indicates that smaller ZnS particles were formed through DBD plasma preparation. The TEM images confirm that the plasma approach generates smaller particles (Fig. 4). As pointed by Anpo et al.[26], small nanoparticles with poor crystallinity favor the migration of generated charges from bulk to the surface over short distance, which is regarded as a key factor for the acceleration of photocatalytic activity. Moreover, smaller particles inevitably increase the active phase dispersion and provide more reactive sites for the reactants than aggregated particles. However, for the thermally-prepared samples, when particle agglomeration appeared after heat treatment, the probability of electron-hole recombination was increased, resulting in a reduced catalytic efficiency.

**Table 1** BET surface area, particle size and band gap of the samples

| Catalyst | BET surface area ($m^2$/g) | Particle size (nm) | Band gap (eV) |
|---|---|---|---|
| CdS/$Al_2O_3$ (CTS) | 205 | 10.7 | 2.28 |
| CdS/$Al_2O_3$ (TS) | 221 | 10.5 | 2.32 |
| CdS/$Al_2O_3$ (CPS) | 216 | 8.1 | 2.35 |
| CdS/$Al_2O_3$ (PS) | 232 | 6.7 | 2.39 |
| ZnS/$Al_2O_3$ (CTS) | 213 | 10.0 | 3.39 |
| ZnS/$Al_2O_3$ (TS) | 227 | 9.7 | 3.43 |
| ZnS/$Al_2O_3$ (CPS) | 231 | 7.5 | 3.52 |
| ZnS/$Al_2O_3$ (PS) | 240 | 6.2 | 3.59 |

From the $N_2$ adsorption isotherms, BET specific surface areas were calculated (Table 1). CdS/$Al_2O_3$ (CTS) possessed the lowest surface area (205 $m^2$/g), whereas CdS/$Al_2O_3$ (PS) showed the highest surface area (232 $m^2$/g). Similarly, the surface area was 213 $m^2$/g for ZnS/$Al_2O_3$ (CTS), and 240 $m^2$/g for ZnS/$Al_2O_3$ (PS). The plasma method can improve the specific surface area of the supported metal sulfides, indicating that plasma can enhance the dispersion of metal sulfide particles. For the plasma-prepared sample, probably due to the short plasma treatment time, the sintering of metal sulfide that occurs in the long-time conventional calcination and thermal sulfidation is avoided. Therefore, a higher specific surface area was obtained by the plasma process, which benefits the good performance in catalysis.

### 3.2 UV-vis analysis

The UV–vis absorption spectra of the samples are presented in Fig. 3. Compared with the spectra of the metal nitrates and metal oxides, it is confirmed that the precursors are transformed into metal sulfides by different methods. Furthermore, plasma-prepared CdS/$Al_2O_3$ and ZnS/$Al_2O_3$ show a significant blue shift in the band gap absorption edge, which may be explained in terms of the size effects that emerge in semiconductors at small particle size. The electrons confined in the nanoparticle exhibit a different behaviour from that in the bulk materials. The properties of the electrons in small semiconductors are dependent upon the crystallite size and the shape due to motion of the electron and hole in a confined space.[26] The relationship of the absorption coefficient and the incident photon energy of semiconductor can be estimated by the Kubelka–Munk equation:[27,28]

$$\alpha(h\nu)=C(h\nu- Eg)^{n/2}$$

where α is the absorption coefficient and its value can be obtained by the equation: $\alpha = (1-R)^2/2R$, R is the diffuse reflectance and its relationship with absorbance can be defined by $R = 10^{-A}$, A is absorbance. h is Planck's constant, ν is frequency, and C is a constant. For a direct transition semiconductor, n = 1; for an indirect transition semiconductor, n = 4. The nature of transition is possible to be determined through plotting the graph of $(\alpha h\nu)^2$ versus hν, thereby the band gap energies can be deduced by extrapolating the straight-linear portions of the plot to intersect the photon energy axis. As a result of the size effect, the band gap of the semiconductor becomes larger with decreasing particle size, and this is indicated by an absorption shift to shorter wavelengths (Table 1). Zhang et al.[29] suggested that volume recombination of the charge carriers is the dominant process in large particles, and can be reduced by a decrease in particle size. This decrease also leads to an increase in the surface area which can be translated as an increase in the available surface active sites. Because of the decrease in particle size, the concentration of unsaturated surface sites such as corners or edges increases, and photon energies absorbed by the catalyst contribute more effectively to the surface reactions. Therefore, the smaller the particle size of the catalyst, the higher the efficiency of photoreaction.

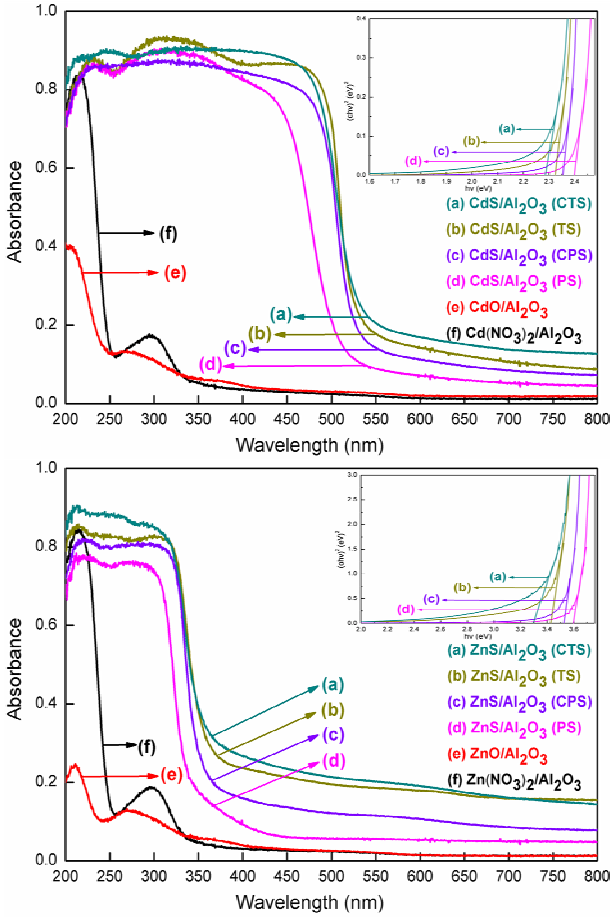


**Fig. 3** UV-vis diffuse reflection spectra for CdS/$Al_2O_3$ and ZnS/$Al_2O_3$ synthesized with different sulfidation methods.

### 3.3 TEM observation

For a better observation of the active phase particle size and

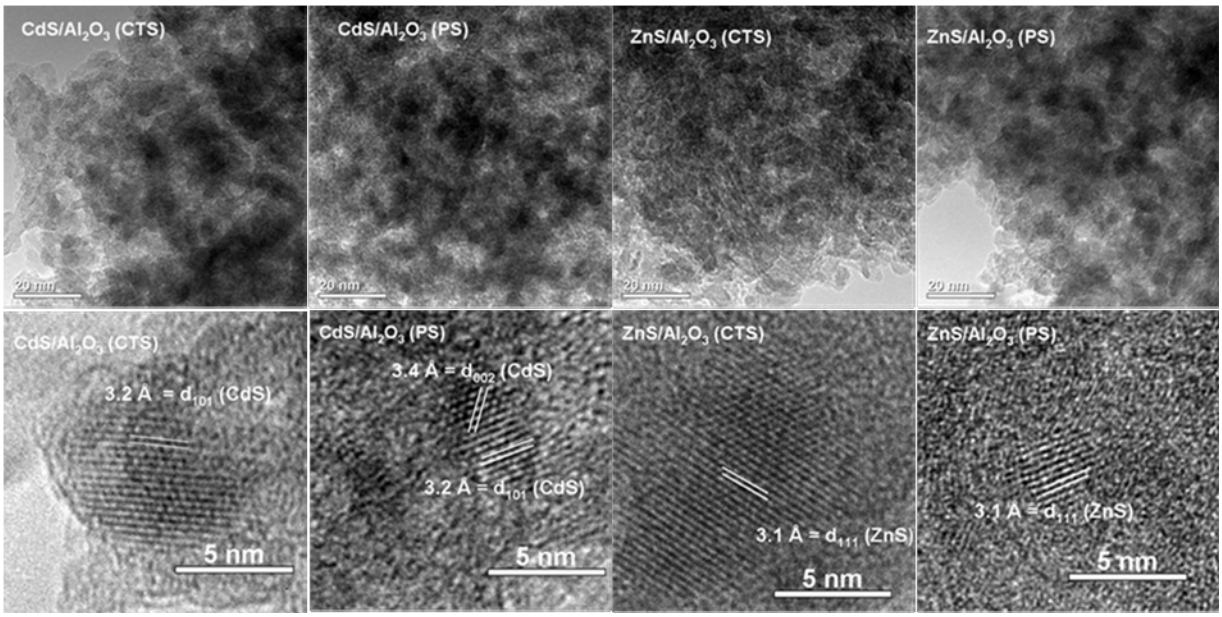


**Fig. 4** TEM images of $CdS/Al_2O_3$ and $ZnS/Al_2O_3$ prepared by different methods (CTS and PS).

morphology, the TEM images of $CdS/Al_2O_3$ and $ZnS/Al_2O_3$ prepared by two different methods are displayed in Fig. 4. For the $CdS/Al_2O_3$ (PS) sample, higher CdS dispersion and smaller particle size were obtained, and no obvious sintering and conglomeration was observed. The lattice fringes of $CdS/Al_2O_3$ (PS) with the interlayer spacing of about 3.2 Å and 3.4 Å correspond to the (101) and (002) planes of CdS (JCPDF No. 060314), respectively. The TEM images of $ZnS/Al_2O_3$ (PS) also suggest that the nanoparticles were well crystallized and the lattice spacing of 3.1 Å is interpreted as $d_{111}$ of ZnS (JCPDF No. 650309). Compared with the thermally prepared samples, the CdS and ZnS clusters of the plasma-prepared ones were smaller and more uniform. The diameter of CdS and ZnS clusters in the plasma-prepared catalysts was about 5 nm, whereas it was about 10 nm for the thermally prepared ones. These results are in agreement with those of XRD characterization.

### 3.4 XPS analysis

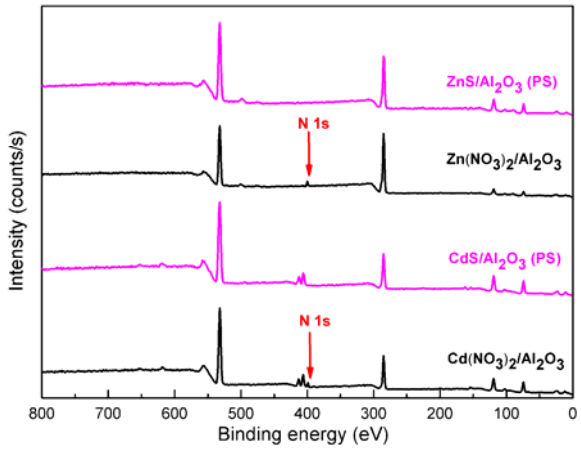


**Fig. 5** XP spectra of $Cd(NO_3)_2/Al_2O_3$, $Zn(NO_3)_2/Al_2O_3$, $CdS/Al_2O_3$ (PS) and $ZnS/Al_2O_3$ (PS).

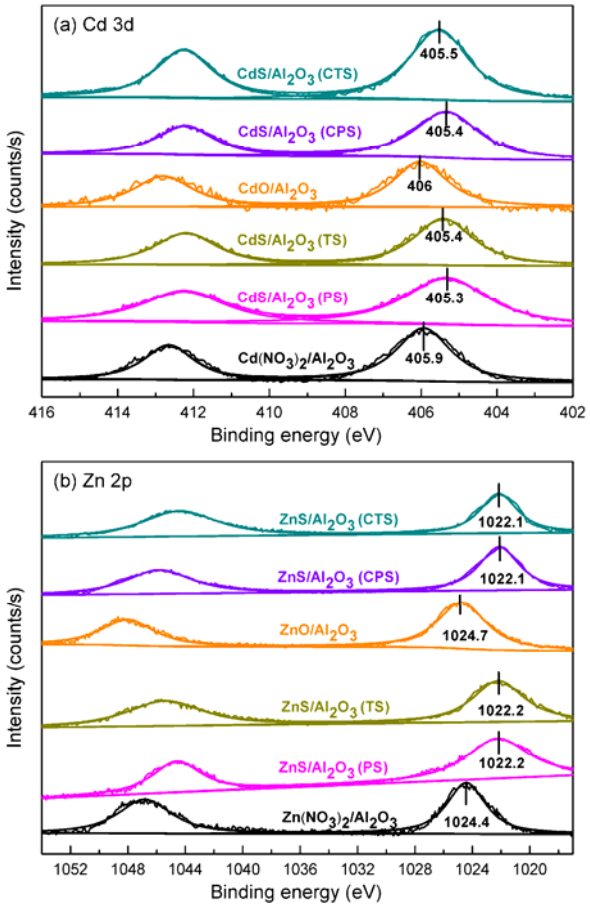


**Fig. 6** XP spectra of $CdS/Al_2O_3$ and $ZnS/Al_2O_3$ synthesized with different preparation methods. (a) XP spectrum of Cd 3d; (b) XP spectrum of Zn 2p.

$Cd(NO_3)_2$ and $Zn(NO_3)_2$ over $Al_2O_3$ were decomposed in the

DBD plasma treatment (Fig. 1). As seen from Fig. 5, the N1s peak at 400 eV assigned to $NO_3^-$ was present initially, but undetectable after the plasma treatment. Fig. 6 shows that the Cd 3d peak of $Cd(NO_3)_2$ at 405.9 eV was shifted to 405.3 eV, which is assigned to the peak of CdS, after the $H_2S$ plasma treatment. Similarly, the Zn 2p peak of $Zn(NO_3)_2$ (1024.4 eV) was shifted to lower binding energy (1022.2 eV), which can be assigned to the peak of ZnS. These results suggest that $Cd(NO_3)_2$ and $Zn(NO_3)_2$ were completely decomposed and then sulfided into CdS and ZnS with the $H_2S$ plasma treatment. In the XP spectra of metal oxides, the Cd 3d peak at 406 eV and the Zn 2p peak at 1024.7 eV can be ascribed to the oxidation states of CdO and ZnO. The shifts of Cd 3d and Zn 2p peaks indicate that metal oxides had been sulfided to CdS and ZnS after sulfidation. In addition, no noticeable differences in the binding energies of Cd 3d, Zn 2p, and S 2p (Fig. S3, ESI†) were found in metal sulfides samples. The Cd 3d peaks at 405.3 eV to 405.5 eV and the Zn 2p peaks at 1022.1 eV and 1022.2 eV could all be indexed to the chemical forms of CdS and ZnS.[30]

**Table 2** The total and surface S/Cd and S/Zn atomic ratios of catalysts with different preparation methods

| Catalyst | Total and surface S/Cd and S/Zn atomic ratios | | | |
|---|---|---|---|---|
| | S/Cd [a] | S/Cd [b] | S/Zn [a] | S/Zn [b] |
| $CdS/Al_2O_3$ (CTS) | 1.00 | 0.96 | — | — |
| $CdS/Al_2O_3$ (TS) | 1.01 | 1.01 | — | — |
| $CdS/Al_2O_3$ (CPS) | 1.01 | 1.10 | — | — |
| $CdS/Al_2O_3$ (PS) | 1.02 | 1.11 | — | — |
| $ZnS/Al_2O_3$ (CTS) | — | — | 1.03 | 0.97 |
| $ZnS/Al_2O_3$ (TS) | — | — | 0.96 | 1.06 |
| $ZnS/Al_2O_3$ (CPS) | — | — | 1.03 | 1.07 |
| $ZnS/Al_2O_3$ (PS) | — | — | 1.06 | 1.10 |

[a] by ICP and elemental analysis, [b] by XPS.

The surface compositions from XPS analysis are summarized in Table S1 (ESI†), together with the bulk composition determined by ICP and elemental analysis. The bulk and surface S/Cd and S/Zn atomic ratios of the supported metal sulfides prepared by different methods are displayed in Table 2. It is shown that the bulk atom ratios of S/Cd and S/Zn were all close to unity, suggesting that the sulfidation degree for all the samples were complete. XPS results reveal that the surface S/Cd and S/Zn atomic ratios for the samples were also close to unity, indicating the formation of CdS and ZnS on the catalyst surface. The S/Cd and S/Zn atomic ratios were slightly higher for plasma-sulfided samples ($CdS/Al_2O_3$ (PS), $CdS/Al_2O_3$ (CPS), $ZnS/Al_2O_3$ (PS), and $ZnS/Al_2O_3$ (CPS)) than for their counterparts. The presence of a small amount of excess sulfur may be related with sulfur deposit on the surface, which is formed by $H_2S$ decomposition during sulfiding process.[31]

### 3.5 Catalytic decomposition of hydrogen sulfide

Hydrogen sulfide ($H_2S$) is a waste gas, but a potential source of hydrogen. Industrial hydrogen production by reforming consumes a large amount of fossil fuels and results in huge emissions of $CO_2$. Production of hydrogen by direct decomposition of $H_2S$ may be an appealing approach to the hydrogen supply in the hydrotreating process in a refinery. We reported that supported metal sulfide semiconductors ($ZnS/Al_2O_3$ and $CdS/Al_2O_3$) worked remarkably together with a DBD plasma in the decomposition of $H_2S$.[20,21] Both electric field and plasma-generated photons are able to excite semiconductor catalysts to generate hole-electron pairs, which played a crucial role in fully converting $H_2S$ to hydrogen and elemental sulfur.

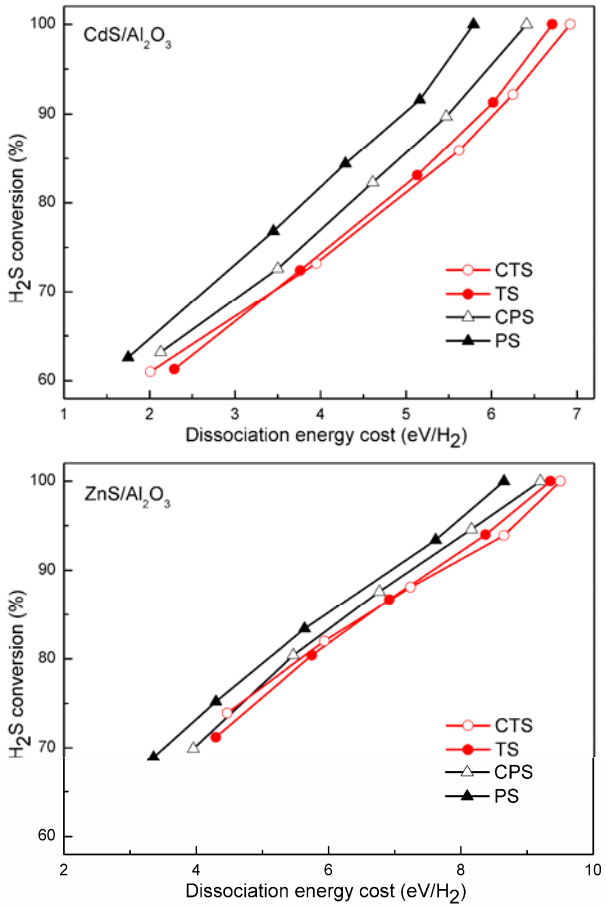


**Fig. 7** $H_2S$ conversion as a function of dissociation energy cost in the plasma-induced decomposition with $CdS/Al_2O_3$ and $ZnS/Al_2O_3$ synthesized by different methods. Reaction conditions: feed: 20% $H_2S$ in Ar; GHSV: 120 $h^{-1}$; catalyst bed volume: 15.0 mL.

Catalytic activities of $CdS/Al_2O_3$ and $ZnS/Al_2O_3$ prepared by different methods in the decomposition of $H_2S$ are compared in Fig. 7. $H_2S$ conversions generally increased with the energy input for all samples. At the same dissociation energy cost, $H_2S$ conversion increased in the following order: CTS ≈ TS < CPS < PS. At an energy consumption of 5.79 eV/$H_2$, $H_2S$ conversions were 100%, 93.2%, 89.2%, and 87.6%, when $CdS/Al_2O_3$ (PS), $CdS/Al_2O_3$ (CPS), $CdS/Al_2O_3$ (TS), and $CdS/Al_2O_3$ (CTS) were filled in the gap, respectively. $ZnS/Al_2O_3$ (PS) promoted the decomposition of $H_2S$ in a similar way, achieving full conversion of $H_2S$ at an energy consumption of 8.64 eV/$H_2$. At this energy cost, the corresponding conversions over the $ZnS/Al_2O_3$ (CPS), $ZnS/Al_2O_3$ (TS), and $ZnS/Al_2O_3$ (CTS) were 97.2%, 95.8%, and 93.9%, respectively. Due to the small difference of properties, the two samples prepared by thermal methods (TS and CTS) showed similar catalytic activity. This was in agreement with the

characterization results. The plasma-sulfided catalysts (PS and CPS) exhibited better catalytic performance compared to the conventional ones. Especially $CdS/Al_2O_3$ (PS) and $ZnS/Al_2O_3$ (PS) pellets showed the highest $H_2S$ decomposition activities among their counterparts. In addition, the conversion variations in $H_2S$ decomposition over $CdS/Al_2O_3$ (PS) and $ZnS/Al_2O_3$ (PS) in the 100 h long-term tests (Fig. S4, ESI†) indicated that the performances of catalysts prepared by $H_2S$ plasma were stable.

The plasma-sulfided catalysts with particle size less than 9 nm showed the higher $H_2S$ conversion. The small particle size can improve the catalytic activity due to the larger specific surface area and active phase dispersion, which provides more active sites and less-perfect crystal lattice with a large number of vacancies to adsorb and activate gaseous reactants. Meanwhile, both the electrons and holes can reach the catalyst surface within a shorter period than in the bulk sample, which is more efficient for the charge separation and transfer. Zou et al.[25] reported that supported NiO catalysts prepared in a non-thermal plasma showed higher activity for photocatalytic water splitting than those obtained with the traditional thermal method. They attributed this enhancement to smaller particle size.

Compared with the counterparts, $CdS/Al_2O_3$ (PS) showed more significant improvement in $H_2S$ conversion than $ZnS/Al_2O_3$ (PS). The reason is probably that the generated $h^+$ and $e^-$ on CdS and ZnS are reactive enough to convert $H_2S$ to $H_2$ and S, and the rate of $H_2S$ decomposition will depend on the population of $h^+$–$e^-$ pairs. Electrons in a larger band gap catalyst require more energy to jump to the conduction band (CB) from the valence band (VB). As a result, the $h^+$–$e^-$ pair population on larger band gap catalysts is lower under a specific electric field and light intensity. With a larger band gap, the $ZnS/Al_2O_3$ catalysts are more difficult to excite, and, therefore, the improvement of their catalytic activities was not as significant as $ZnS/Al_2O_3$ (PS) catalysts.

## Conclusions

A novel DBD plasma method was employed to prepare supported metal sulfide catalysts. The plasma method not only reduces the preparation time but also achieves an increased dispersion, small sulfide cluster size, and uniform distribution, compared to the traditional thermal method. The plasma-prepared $CdS/Al_2O_3$ and $ZnS/Al_2O_3$ catalysts exhibited an enhanced performance for hydrogen production from plasma-induced $H_2S$ decomposition at reduced energy cost. The enhancement might be attributed to the smaller particle size, higher surface area and dispersion. This technique is also applicable to the synthesis of other supported metal sulfides, such as CoS, $FeS_2$, $Ag_2S$, MnS, NiS, $MoS_2$, CuS, and $WS_2$.

## Acknowledgments

This work was financially supported by NSFC (20503003, 20773020, 20973030, 21173033, U1162203), The Ph.D. Programs Foundation (MOE, 20100041110016), NCET (04-0275), and the “863” Project (2008AA030803).

## References

1 C. H. Lai, M. Y. Lu and L. J. Chen, *J. Mater. Chem.*, 2012, **22**, 19.
2 G. Henshaw, I. P. Parkin and G. Shaw, *Chem. Commun.*, 1996, 1095.
3 S. Biswas, A. Mondal, D. Mukherjee and P. Pramanik, *J. Electrochem. Soc.*, 1986, 1**33**, 48.
4 S. H. Yu, J. Yang, Y. S. Wu, Z. H. Han, Y. Xie and Y. T. Qian, *Mater. Res. Bull.*, 1998, **33**, 1661.
5 S. H. Yu, Y. T. Qian, L. Shu, Y. Xie, L. Yang and C. S. Wang, *Mater. Lett.*, 1998, **35**, 116.
6 P. Matteazzi and G. Le Caër, *Mater. Sci. Eng., A*, 1992, **156**, 229.
7 J. J. Zhu, S. W. Liu, O. Palchik, Y. Koltypin and A. Gedanken, *J. Solid State Chem.*, 2000, **153**, 342.
8 D. Routkevitch, T. Bigioni, M. Moskovits and J. M. Xu, *J. Phys. Chem.*, 1996, **100**, 14037.
9 I. Jen-La Plante, T. W. Zeid, P. D. Yang and T. Mokari, *J. Mater. Chem.*, 2010, **20**, 6612.
10 E. Furimsky, *Appl. Catal., A*, 1998, **171**, 177.
11 D. R. Huntley, *Surf. Sci.*, 1990, **240**, 13.
12 R. I. R. Blyth, C. Searle, N. Tucker, R. G. White, T. K. Johal, J. Thompson and S. D. Barrett, *Phys. Rev. B*, 2003, **68**, 205404.
13 X. L. Zhu, P. P. Huo, Y. P. Zhang and C. J. Liu, *Ind. Eng. Chem. Res.*, 2006, **45**, 8604.
14 J. H. He, I. Ichinose, T. Kunitake and A. Nakao. *Langmuir*, 2002, **18**, 10005.
15 W. Chu, L. N. Wang, P. A. Chernavskii and A. Y. Khodakov, *Angew. Chem. Int. Ed.*, 2008, **47**, 5052.
16 J. P. Hong, W. Chu, P. A. Chernavskii and A. Y. Khodakov, *J. Catal.*, 2010, **273**, 9.
17 G. H. Liu, Y. L. Li, W. Chu, X. Y. Shi, X. Y. Dai and Y. X. Yin, *Catal. Commun.*, 2008, **9**, 1087.
18 W. Hua, L. J. Jin, X. F. He, J. H. Liu and H. Q. Hu, *Catal. Commun.*, 2010, **11**, 968.
19 A. J. Wang, M. L. Qin, J. Guan, L. Wang, H. C. Guo, X. Li, Y. Wang, R. Prins and Y. K. Hu, *Angew. Chem. Int. Ed.*, 2008, **47**, 6052.
20 L. Zhao, Y. Wang, L. Jin, M. L. Qin, X. Li, A. J. Wang, C. S. Song and Y. K. Hu, *Green Chem.*, 2013, **15**, 1509.
21 L. Zhao, Y. Wang, X. Li, A. J. Wang, C. S. Song and Y. K. Hu, *Int. J. Hydrogen Energy*, 2013, **38**, 14415.
22 H. H. Kim, Y. H. Lee, A. Ogata and S. Futamura, *Catal. Commun.*, 2003, **4**, 347.
23 A. Fridman, *Plasma Chemistry*, Cambridge University Press, New York, 2008, Ch. 10, p. 744.
24 C. J. Liu, J. J. Zou, K. L. Yu, D. G. Cheng, Y. Han, J. Zhan, C. Ratanatawanate and B. W. L. Jang, *Pure Appl. Chem.*, 2006, **78**, 1227.
25 J. J. Zou, C. J. Liu and Y. P. Zhang, *Langmuir*, 2006, **22**, 2334.
26 M. Anpo, T. Shima, S. Kodama and Y. Kubokawa, *J. Phys. Chem.*, 1987, **91**, 4305.
27 M. A. Butler, *J. Appl. Phys.*, 1977, **48**, 1914.
28 K. Domen, A. Kudo and T. Onishi, *J. Catal.*, 1986, **102**, 92.
29 Z. B. Zhang, C. C. Wang, R. Zakaria and J. Y. Ying, *J. Phys. Chem. B.*, 1998, **102**, 10871.
30 C. D. Wanger, W. M. Riggs, L. E. Davis, J. F. Moulder and G. E. Muilenberg, *Handbook of X-ray Photoelectron Spectroscopy*, Physical Electronics Division, Minnesota, 1979, p. 171.
31 I. Karamé, *Hydrogenation*, In Tech Press, Rijeka, 2012, Ch. 9, p. 236.

## Entry for the Table of Contents

**Synthesis of highly dispersed metal sulfide catalysts via low temperature sulfidation in a dielectric barrier discharge plasma**

Lu Zhao, Yao Wang*, Zhili Sun, Anjie Wang, Xiang Li, Chunshan Song and Yongkang Hu

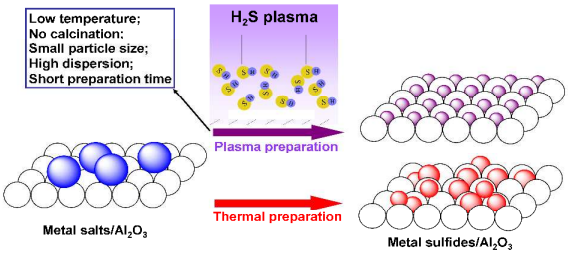


Highly dispersed metal sulfide catalysts were synthesized by low temperature sulfidation in a non-thermal plasma directly from the metal salts.